Received: 3 May 2018 | Revised: 18 June 2018 | Accepted: 25 June 2018
DOI: 10.4218/etrij.2018-0220

ORIGINAL ARTICLE

WILEY ETRI Journal

Compact tri-wideband bandpass filter with multiple transmission zeros

Yang Xiong[1] | LiTian Wang[2] | Li Gong[2] | KaiYong He[2] | Man Zhang[2] | Hui Li[2] | XinJie Zhao[2]

[1]The Southwest China Institute of Electronic Technology, Chengdu, China.
[2]College of Electronic Information and Optical Engineering, Nankai University, Tianjin, China.

Correspondence
LiTian Wang, College of Electronic Information and Optical Engineering, Nankai University, Tianjin, China.
Email: wanglitianrf@sina.com

Funding information
Nankai University; National Natural Science Foundation of China, Grant/Award Number: 61101018, 51002081, 61171028.

This paper presents a tri-wideband bandpass filter (TWB-BPF) with compact size, high band-to-band isolation, and multiple transmission zeros (TZs). The proposed TWB-BPF is based on a multiple-mode resonator (MMR), which is interpreted by the method of the even- and odd-mode analysis technique. The MMR can excite 11 resonant modes, where the first two modes comprise the first passband, the next four modes form the second passband, and the last five modes are used to generate the third passband. In addition, 10 TZs are yielded to obtain high band-to-band isolation and wide stopband suppression characteristics up to $14.95f_{c1}$ (f_{c1} is the center frequency of the first passband). To verify the proposed filter, a TWB-BPF with 3-dB fractional bandwidths (FBWs) of 37.4%, 43.5%, and 40.4% is designed, fabricated, and measured.

KEYWORDS
bandpass filter, multi-mode resonator, transmission zeros, tri-wideband, wide stopband

1 | INTRODUCTION

To meet the requirements of high data rate, high transmission capacity, and multiple services in modern communication systems, there have been accelerated developments to realize radio-frequency (RF) front-ends that are multi-band and broadband. In recent years, multi-band bandpass filters (BPFs) have attracted much interest. For example, various excellent works that focused mainly on multi-band and high selectivity have been reported [1–17]. In [1–5], step-impedance resonators are widely employed to design dual-band, tri-band, and quad-band BPFs. The method of combining several BPFs or resonators with common input/output ports is a straightforward and effective approach to design multi-band BPFs [6–9]. Using this approach, single-band, dual-band, tri-band, quad-band, and quint-band BPFs can be easily achieved [6]. In [10,11], the concept of signal multipath transmission is used to design high-performance tri-band BPFs. Owing to the merits of their simple structure and controllable resonant frequencies, multiple-mode resonators (MMRs) are also widely used to design multi-band BPFs [12–18]. In [12], a very closely spaced passband and highly selective dual-band BPF are developed using MMR. Although the filters [1,3–6,8–14,18] have demonstrated their high performances, the narrow bandwidth is still insufficient to meet the requirements of broadband wireless communication systems. To solve this issue, several dual-/tri-wideband BPFs were developed to satisfy those requirements. The 3-dB fractional bandwidths (FBWs) of these reported multi-wideband BPFs are mainly about 10%–20%, while a TWB-BPF with 3-dB FBWs >40% is occasionally reported. Moreover, the notch-like stopband characteristics of these multi-wideband BPFs need to be further improved.

In this paper, a compact TWB-BPF based on a novel MMR, which is interpreted using the even- and odd-mode analysis method, is presented. The filter has a high band-to-band isolation and wide stopband suppression characteristics up to $14.95f_{c1}$. The center frequencies (CFs) of the TWB-

BPF are 1.07 GHz, 3.25 GHz, and 8.32 GHz with 3-dB FBWs of 37.4%, 43.5%, and 40.4%, respectively. To verify these results, a TWB-BPF with compact size, high band-to-band isolation, and wide upper stopband suppression was designed, fabricated, and measured. The measured and full-wave electromagnetic simulated results of the TWB-BPF agree well with each other.

2 | DESIGN Of TWB-BPF

Figure 1 shows the configuration of the proposed MMR, which consists of a cross-shaped resonator (denoted by (L_1, W_1), (L_3, W_3), (L_4, W_4), and (L_5, W_5)) with shorted circuit termination, and two sets of symmetrical stub-loaded resonators (denoted by (L_2, W_2) (L_6, W_6), and (L_7, W_7)). Figure 1A shows the layout of the proposed TWB-BPF. Figure 1B illustrates the transmission-line model (TLM) of the TWB-BPF. Considering that the structure is symmetrical with the T-T' plane, the even- and odd-mode analysis technique was employed to analyze this MMR. Figure 1C and D, respectively, show the odd-mode and even-mode equivalent circuits.

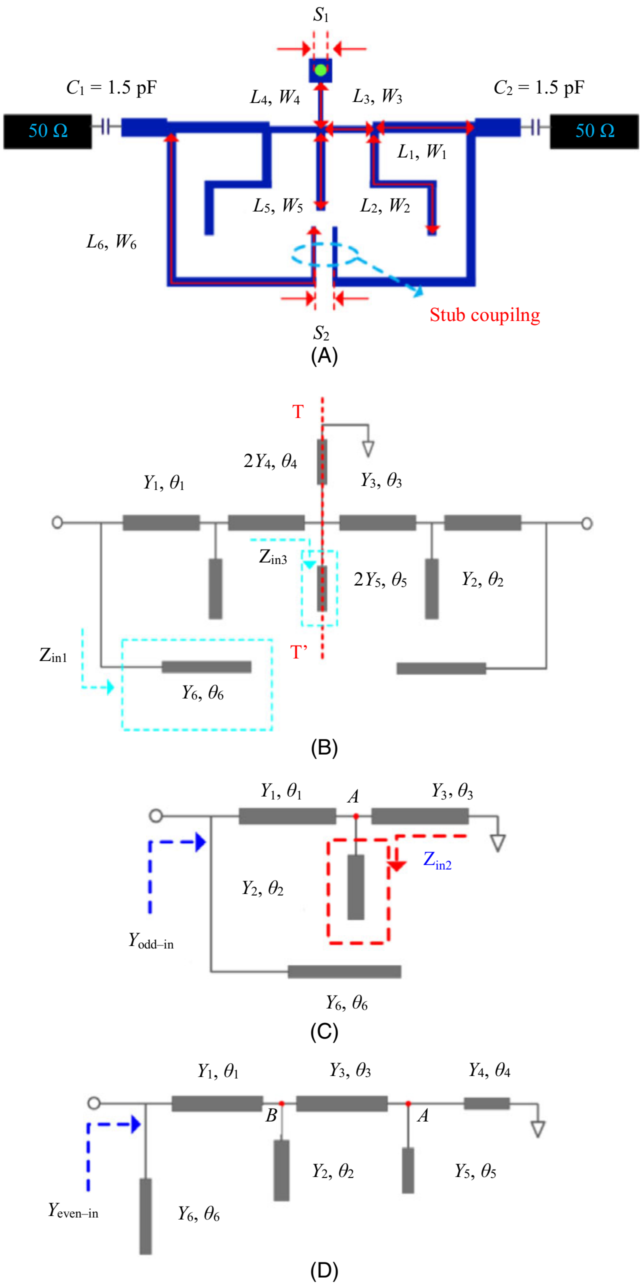

FIGURE 1 Proposed TWB-BPF (A) layout, (B) TLM, (C) odd-mode equivalent circuit, and (D) even-mode equivalent circuit

As illustrated in Figure 1C, $Y_{\text{odd-in}}$ denotes the input admittance under odd-mode excitation. Likewise, $Y_{\text{even-in}}$ represents the input admittance under even-mode excitation, as shown in Figure 1D. For simplicity, the parameter L_7 is neglected. According to the transmission-line theory, we can derive the following results.

$$Y_{\text{odd-in}} = \frac{Y_1(Y_{\text{in}A} + \text{j}Y_1\tan\theta_1)}{Y_1 + \text{j}Y_{\text{in}A}\tan\theta_1} + \text{j}Y_6\tan\theta_6, \tag{1}$$

$$Y_{\text{in}A} = j(Y_2\tan\theta_2 - Y_3\cot\theta_3), \tag{2}$$

$$Y_{\text{even-in}} = \frac{Y_1(Y_{\text{in}B} + \text{j}Y_1\tan\theta_1)}{Y_1 + \text{j}Y_{\text{in}B}\tan\theta_1} + \text{j}Y_2\tan\theta_2, \tag{3}$$

$$Y_{\text{in}B} = \frac{Y_3(Y_{\text{in}A} + \text{j}Y_3\tan\theta_3)}{Y_3 + \text{j}Y_{\text{in}A}\tan\theta_3} + \text{j}Y_2\tan\theta_2, \tag{4}$$

$$Y_{\text{in}A} = j(Y_5\tan\theta_5 - Y_4\cot\theta_4), \tag{5}$$

where Y_n (n = 1, 2, 3, 4, 5, and 6) and θ_n (n = 1, 2, 3, 4, 5, and 6) represent the characteristic admittance and electrical length, respectively. For simplicity, we let the center frequency $f_0 = 2.4$ GHz (reference frequency for electrical length calculation), $Y_3 = 1/160$ S, $Y_1 = Y_2 = Y_4 = Y_5 = Y_6 = 0.01$ S. According to the resonant condition, we have:

$$\text{Im}(Y_{\text{odd-in}}) = 0, \tag{6}$$

$$\text{Im}(Y_{\text{even-in}}) = 0. \tag{7}$$

As an example, the circuit parameters are set as $\theta_1 = 45°$, $\theta_2 = 47°$, $\theta_3 = 10°$, $\theta_4 = 7°$, $\theta_5 = 21°$, $\theta_6 = 106°$, $Z_1 = Z_2 = Z_4 = Z_5 = Z_6 = 100$ Ω, $Z_3 = 80$ Ω, and Z_n (n = 1, 2, 3, 4, 5, and 6) denote the characteristic impedance. Therefore, the resonant frequencies can be solved numerically based on (6) and (7).

In detail, the initial circuit parameter values of the electrical lengths are calculated at f_0. When a certain frequency f_i is considered, the values of the electrical lengths can be redefined as $\theta_n^* = \theta_n f_i/f_0$ (n = 1, 2, 3, 4, 5, and 6). Then, we substitute the updated values of the electrical lengths into (1–7). For example, if (6) is satisfied, it means that f_i is an odd-mode resonant frequency for which we are searching.

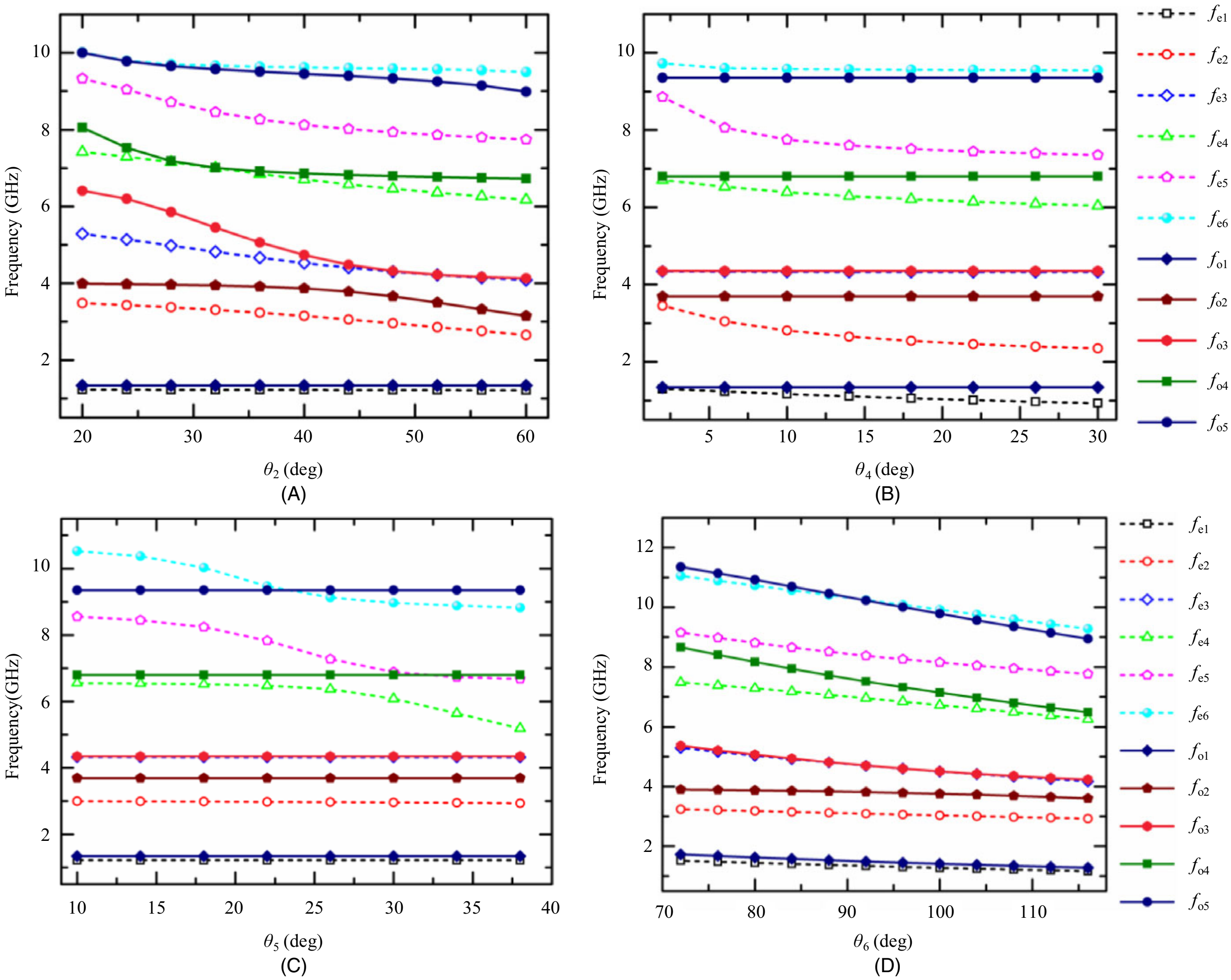

FIGURE 2 Properties of resonance frequencies vs (A) θ_2, (B) θ_4, (C) θ_5, and (D) θ_6

As shown in Figure 2, we investigate the resonant frequencies of the MMR vs various values of θ_2, θ_4, θ_5, and θ_6. As can be seen, 11 resonant modes have been excited, where f_{o1}, f_{o2}, f_{o3}, f_{o4}, and f_{o5} denote the odd-mode resonant frequencies determined by (6), whereas f_{e1}, f_{e2}, f_{e3}, f_{e4}, f_{e5}, and f_{e6} represent the even-mode resonant frequencies determined by (7). It can be observed from Figure 2A that f_{ei} (i = 2, 3, 4, 5, 6) and f_{oi} (i = 2, 3, 4, 5) decrease with the increase in θ_2, whereas f_{o1} and f_{e1} change slightly. As shown in Figure 2B, θ_4 mainly affects the resonant frequencies of f_{ei} (i = 1, 2, 4, 5, 6) with f_{oi} (i = 1, 2, 3, 4, 5) unchanged. As illustrated in Figure 2C, f_{e4}, f_{e5}, and f_{e6} decrease dramatically, whereas the others resonant frequencies remain unchanged with the increase in θ_5. As shown in Figure 2D, the 11 resonant frequencies decrease with the increase in θ_6.

As illustrated in Figure 3, the frequency responses of the TWB-BPF are simulated using TLM. It can be

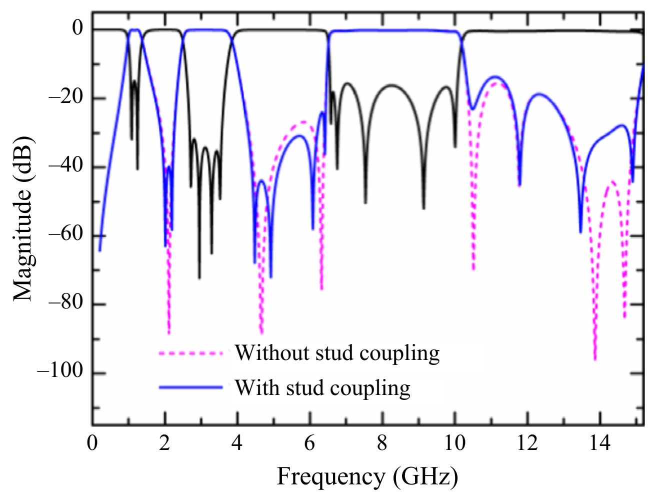

FIGURE 3 Simulated results of frequency responses with and without stub coupling

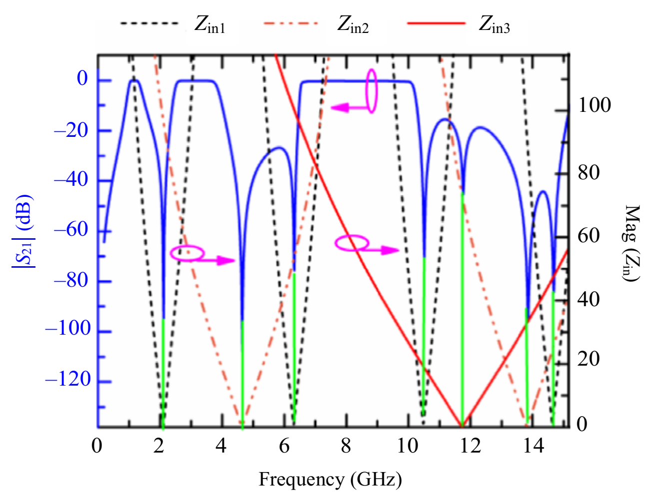

FIGURE 4 Frequency responses of $|S_{21}|$ and Z_{in}

observed that the filter has 11 transmission poles (TPs), where the first two poles compose the first passband, the next four poles form the second passband, and the last five poles are used to construct the third one. It can be observed that three additional TZs are generated by introducing stub coupling. In order to determine how the TZs are generated, the relationship between TZ and Z_{in} is investigated, as shown in Figure 4. It can be found that a TZ will be generated at a certain frequency, where $Z_{in} = 0$ is satisfied. This is attributed to the introduction of virtual ground to short out the transmission signals. Finally, the condition for the generation of TZs can be expressed as:

$$Z_{in1} = -jZ_6 \cot\theta_6 = 0, \quad (8)$$

$$Z_{in2} = -jZ_2 \cot\theta_2 = 0, \quad (9)$$

$$Z_{in3} = -jZ_5 \cot\theta_5 = 0. \quad (10)$$

That is,

$$f_{TZ} = \frac{(2n+1)c}{4L_6\sqrt{\varepsilon_{re}}} \quad (n = 0,\ 1,\ 2,\ \ldots), \quad (11)$$

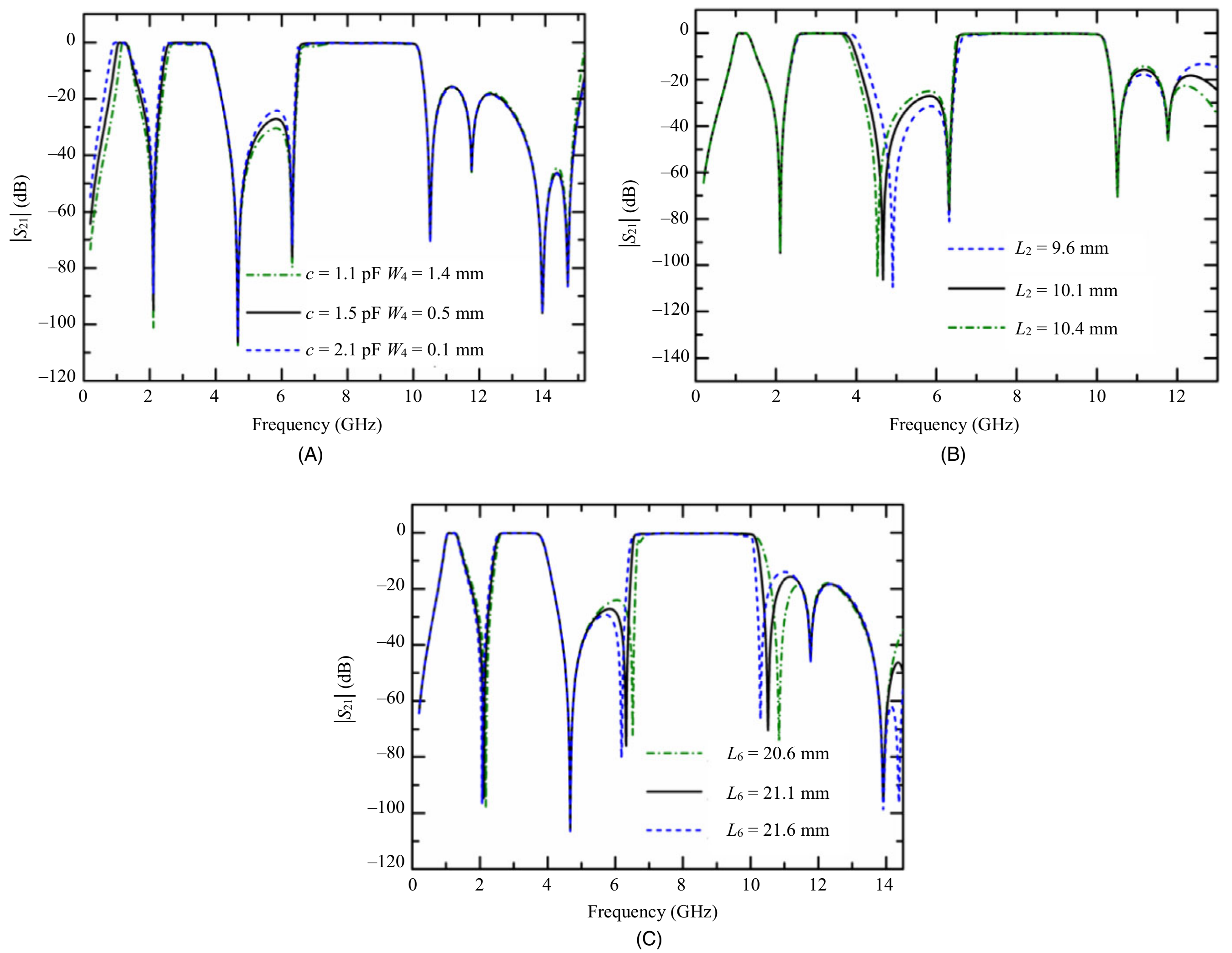

FIGURE 5 Resonance properties vs (A) capacitance and W_4, (B) L_2, (c) L_6

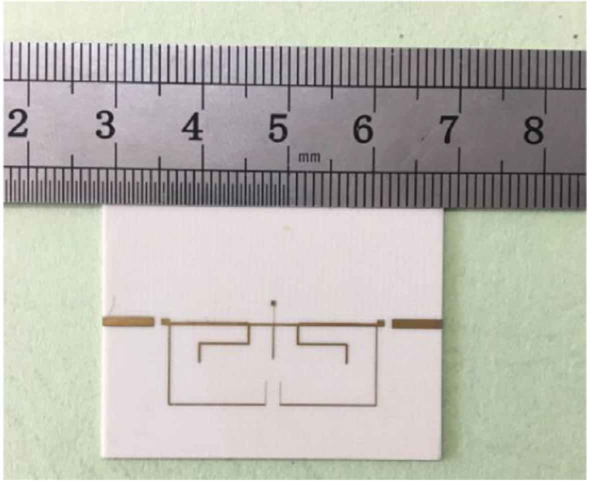

(A)

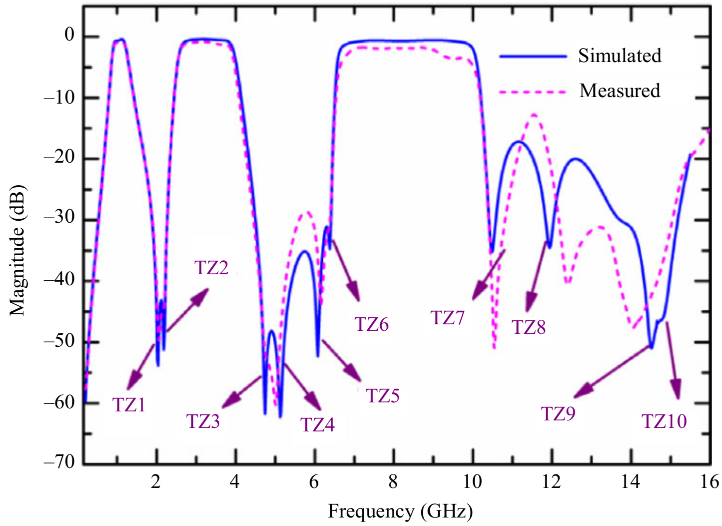

(B)

FIGURE 6 (A) Photograph of the fabricated TWB-BPF, (B) simulated and measured results of the TWB-BPF

$$f_{TZ} = \frac{(2n+1)c}{4L_2\sqrt{\varepsilon_{re}}} \quad (n = 0,\ 1,\ 2,\ \ldots), \tag{12}$$

$$f_{TZ} = \frac{(2n+1)c}{4L_5\sqrt{\varepsilon_{re}}} \quad (n = 0,\ 1,\ 2,\ \ldots). \tag{13}$$

As shown in Figure 5A, the first passband can be adjusted by tuning the capacitance and W_4, while the second and third passbands remain almost unchanged. Figure 5B shows that the second passband can be shifted by changing L_2. Furthermore, the variation in L_2 does not affect the other passbands. Figure 5C shows that L_6 only affects the third passband.

3 | EXPERIMENTAL VERIFICATION

For validation, a TWB-BPF was fabricated on a substrate of Rogers 4003 with parameters: $\varepsilon_r = 3.38$, $h = 0.508$ mm, and tan $\delta = 0.0027$. The physical dimensions of this BPF were optimized by Sonnet 15.52, and the parameters are given as $L_1 = 9.3$, $W_1 = 0.45$, $L_2 = 10.3$, $W_2 = 0.3$, $L_3 = 2.9$, $W_3 = 0.3$, $L_4 = 2.1$, $W_4 = 0.1$ $L_5 = 4$, $W_5 = 0.2$, $L_6 = 20.6$, $W_6 = 0.2$, $L_7 = 2.85$, $W_7 = 0.1$, $S_1 = 0.3$, and $S_2 = 1.6$ (unit: mm). The frequency responses of the simulated and measured results are shown in Figure 6. It can be observed that the measured CFs are centered at 1.07 GHz, 3.25 GHz, and 8.32 GHz with 3-dB FBWs of 37.4%, 43.5%, and 40.4%, respectively. The minimum insertion losses (ILs) of the three passbands are 0.75 dB, 0.83 dB, and 1.78 dB, respectively. It can be seen that the maximum band-to-band isolations are about 50 dB and 60.3 dB, respectively. A wide stopband suppression up to $14.95f_{c1}$ with a rejection level of 13 dB was achieved. A comparison between this work and some reported tri-band BPFs is summarized in Table 1, and shows that the TWB-BPF has a low IL, compact size, and broad bandwidth.

4 | CONCLUSION

In this paper, we presented a compact TWB-BPF based on a novel MMR, and its resonant behavior was analyzed.

TABLE 1 Comparison with some reported tri-band BPFs

Filter	CFs (GHz)	3–dB FBWs (%)	ILs (dB)	TPs/TZs	Size ($\lambda_g \times \lambda_g$)
[2]	1.9/5.65/9.2	53/17.7/10.87	3.65/3.65/3.65	6/2	0.694 × 0.076
[3]	1.57/3.9/7	4.1/2/3	2.0/2.1/1.8	6/6	0.145 × 0.113
[7]	2/3.6/5.5	18.5/10.1/13.2	3.0/3.0/3.0	6/6	0.303 × 0.156
[11]	1.575/1.8/2.4	6.1/3.5/3.1	0.7/0.9/0.9	6/6	0.21 × 0.12
[17]	1.25/3.5/6.82	24.4/18.3/13.8	0.45/0.42/1.26	6/7	0.156 × 0.149
This work	1.07/3.25/8.32	37.4/43.5/40.4	0.75/0.83/1.78	11/10	0.166 × 0.073

The proposed TWB-BPF has a wide bandwidth in each passband, a high band-to-band isolation, low IL, and wide stopband suppression, which makes the filter attractive for multiple services and broadband wireless communication systems.

ACKNOWLEDGEMENTS

This work was supported by the Ph.D. Candidate Research Innovation Fund of Nankai University and National Natural Science Foundation of China under Grants (61101018, 51002081, and 61171028).

ORCID

LiTian Wang http://orcid.org/0000-0002-1618-1008

REFERENCES

1. C.-I. G. Hsu, C. H. Lee, and Y. H. Hsieh, *Tri-band bandpass filter with sharp passband skirts designed using tri-section sirs*, IEEE Microw. Wireless Compon. Lett. **18** (2008), no. 1, 19–21.
2. J. P. Hu et al., *A new wideband triple-band filter using sir*, J. Electromagn. Waves Applicat. **25** (2011), no. 16, 2287–2295.
3. J. Li, S. S. Huang, and J. Z. Zhao, *Design of a compact and high selectivity Tri-band bandpass filter using asymmetric stepped-impedance resonators (sirs)*, Prog. Electromagn. Res. Lett. **44** (2014), 81–86.
4. S. B. Zhang and L. Zhu, *Fully canonical dual-band bandpass filter with λ/4 stepped impedance resonators*, Electron. Lett. **50** (2014), no. 3, 192–194.
5. J. K. Xiao et al., *Miniature quad-band bandpass filter with passband individually controllable using folded SIR*, Electron. Lett. **50** (2014), no. 9, 679–680.
6. C. F. Chen, *Design of a compact microstrip quint-band filter based on the tri-mode stub-loaded stepped-impedance resonators*, IEEE Microw. Wireless Compon. Lett. **22** (2012), no. 7, 357–359.
7. H. W. Deng, *Design of compact and high selectivity Tri-band wideband microstrip BPF*, Microw. Opt. Technol. Lett. **55** (2013), no. 2, 258–261.
8. C. F. Chen et al., *Design of compact microstrip sept-band bandpass filter with flexible passband allocation*, IEEE Microw. Wireless Compon. Lett. **26** (2016), no. 5, 346–348.
9. H. W. Liu et al., *Quad-band bandpass filter using quad-mode stub-loaded resonators*, ETRI J. **36** (2014), no. 4, 690–693.
10. S. Yang et al., *Compact and high selectivity tri-band bandpass filter using multipath-embedded resonators*, Prog. Elecromagn. Res. Lett. **50** (2014), 35–40.
11. H. W. Wu et al., *New triple-passband bandpass filter using multipath stub loaded resonators*, IEEE Microw. Wireless Compon. Lett. **26** (2016), no. 3, 186–188.
12. Y. Xiong et al., *Design of dual-band bandpass filter with closely spaced passbands and multiple transmission zeros*, Prog. Electromagn. Res. Lett. **70** (2017), 45–51.
13. H. W. Liu et al., *Compact and high selectivity Tri-band bandpass filter using multimode stepped-impedance resonator*, IEEE Microw. Wireless Compon. Lett. **23** (2013), no. 10, 536–538.
14. S. Liu and J. Xu, *Compact Tri-band bandpass filter using SISRLR*, Electron. Lett. **52** (2016), no. 18, 1539–1541.
15. Y. Xiong et al., *Dual-wideband bandpass filter with independently controllable center frequencies and wide stopband*, Int. J. Microw. Wireless Technol. **10** (2018), no. 1, 93–99.
16. K. C. Lee et al., *A Review of centrally loaded multimode microstrip resonators for bandpass filter design*, Int. J. Electron. Commun. **69** (2015), no. 10, 1533–1540.
17. J. Xu, W. Wu, and C. Miao, *Compact microstrip Dual-/Tri-/Quad-band bandpass filter using open stubs loaded shorted stepped-impedance resonator*, IEEE Trans. Microw. Theory Tech. **61** (2013), no. 9, 3187–3199.
18. J. Xu, W. Wu, and G. Wei, *Compact multi-band bandpass filters with mixed electric and magnetic coupling using multiple-mode resonator*, IEEE Trans. Microw. Theory Tech. **63** (2015), no. 12, 3909–3919.

AUTHOR BIOGRAPHIES

Yang Xiong was born in Huaihua, Hunan province, China, in 1990. He received the BE degree from Shandong University of Technology, Zibo, China, in 2013, and the PhD degree from Nankai University, Tianjin, China, in 2018. His main research interest is microwave circuit design.

LiTian Wang was born in Tianjin, China, in 1991. He is currently working toward the PhD degree at Nankai University, Tianjin, China. His main research interests include microwave passive components and systems, and HTS tunable filter design.

Li Gong was born in Suzhou, Jiangsu province, China. He received the BE degree from Suzhou University of Science and Technology, Suzhou, China, in 2016, and is currently working toward the ME degree at Nankai University, Tianjin, China. His main research interests are microwave filters and multiplexer design.

KaiYong He was born in Chaozhou, Guangdong province, China, in 1996. He is currently working toward the BE degree at Nankai University, Tianjin, China. His main research interest is HTS devices.

Man Zhang received her BE degree in electronic and information engineering from Ocean University of China, Qingdao, China, in 2016, and is currently working toward the ME degree in communication and information system. Her main research interests are microwave filters and multiplexer design.

Hui Li received her BE degree in communication engineering from Liaocheng University, Liaocheng, China, in 2015, and is currently working toward the ME degree in communication and information systems. Her main research interest is microwave filters.

Xinjie Zhao received his ME degree in semiconductor physics from University of the Inner Mongol, Huhehaote, China, in 1988, and his PhD degree in material science from the China Institute of Atomic Energy, Beijing, China, in 1999. Since 2002, he has been a professor with the Department of Electronics, Nankai University, Tianjin, China. His research interests are in the fields of high-temperature superconductor applications, the generation and detection of THz signals, and microwave devices.